Published in final edited form as:
Mol Genet Metab. 2010 April ; 99(4): 408–416. doi:10.1016/j.ymgme.2009.12.005.

A *Pex7* hypomorphic mouse model for plasmalogen deficiency affecting the lens and skeleton

Nancy Braverman[a,*], **Rui Zhang**[b], **Li Chen**[b], **Graeme Nimmo**[a], **Sarah Scheper**[b], **Tammy Tran**[b], **Rupsa Chaudhury**[b], **Ann Moser**[c], and **Steven Steinberg**[c]

[a] Department of Human Genetics and Pediatrics, Montreal Children's Hospital Research Institute, McGill University, Montreal, QC, H3Z 2Z3, Canada

[b] McKusick-Nathans Institute of Genetic Medicine, Johns Hopkins University, Baltimore, MD, 21205, USA

[c] Department of Neurogenetics, Kennedy Krieger Institute, Johns Hopkins University, Baltimore, MD, 21205, USA

Abstract

Rhizomelic chondrodysplasia punctata type 1 is a peroxisome biogenesis disorder with the clinical features of rhizomelia, abnormal epiphyseal calcifications, congenital cataracts, and profound growth and developmental delays. It is a rare autosomal recessive disorder, caused by defects in the peroxisome receptor, Pex7. The pathology results from a deficiency of plasmalogens, a critical class of ether phospholipids whose functions are largely unknown. To study plasmalogens in an animal model, avoid early mortality and facilitate therapeutic investigations in this disease, we engineered a hypomorphic mouse model in which *Pex7* transcript levels are reduced to less than 5% of wild type. These mice are born in expected ratios, are fertile and have a normal life span. However, they are petite and develop early cataracts. Further investigations showed delayed endochondral ossification and abnormalities in lens fibers. The biochemical features of reduced Pex7 function were reproduced in this model, including tissue plasmalogen deficiency, phytanic acid accumulation, reduced import of Pex7 ligands and consequent defects in plasmalogen biosynthesis and phytanic acid oxidation. Dietary supplementation with batyl alcohol, a plasmalogen precursor, recovered ether phospholipids in blood, but did not alter the clinical phenotype. The relatively mild phenotype of these mice mimics patients with milder pex7 defects, and highlights the skeleton and lens as sensitive markers of plasmalogen deficiency. The role of plasmalogens in the normal function of these tissues at various ages can now be studied and additional therapeutic interventions tested in this model.

Keywords

Pex7; mouse models; Peroxisome Biogenesis Disorder; Rhizomelic Chondrodysplasia Punctata; plasmalogens; phytanic acid

*Corresponding author. Fax 514 412 4478, nancy.braverman@mcgill.ca (N. Braverman).

Introduction

1.1 Rhizomelic chondrodysplasia punctata (RCDP)[1] phenotype

RCDP type 1 (RCDP1) is a peroxisome biogenesis disorder with the clinical features of rhizomelia, punctate calcifications in epiphyseal cartilage, congenital cataracts, profound growth and developmental delays. A proportion of infants do not survive the neonatal period, and ~50% of survivors are alive at 5 yrs of age [1,2]. Over time, there is progression of skeletal abnormalities, with metaphyseal flaring, epiphyseal irregularities and spinal stenosis, development of seizures and cerebellar atrophy [3,4]. Respiratory complications are a frequent cause of death.

RCDP1 is caused by defects in *PEX7*, which encodes the receptor for PTS2-targeted peroxisome matrix enzymes, alkyl-dihydroxyacetonephosphate synthase (AGPS, EC 2.5.1.26), phytanoyl-CoA hydroxylase (PhyH, EC 1.14.11.18) and 3-oxoacyl-Coenzyme A thiolase (ACAA1, acetyl-CoA acyltransferase 1, EC 2.3.1.16) [5]. Consequently, these enzymes remain in the cytosol, where they are nonfunctional and degraded. PhyH is required for the α-oxidation of phytanic acid (PA) to 2-hydroxyphytanoyl CoA, which is subsequently converted to pristanic acid and catabolized further by β-oxidation [6]. ACAA1 catalyzes the removal of acetyl-CoA from saturated straight chain acyl-CoA in the last step of β-oxidation. AGPS participates in plasmalogen synthesis by exchanging a fatty acid at the sn-1 position of dihydroxyacetone phosphate with a fatty alcohol, partnering with a second enzyme, GNPAT (EC 2.3.1.42), which is imported into the peroxisome by the PTS1 pathway. AGPS and GNPAT control the rate limiting steps of plasmalogen biosynthesis [6].

The RCDP1 phenotype is uniquely determined by the loss of AGPS activity, resulting in deficient plasmalogen synthesis. This is supported by identical RCDP phenotypes in single enzyme defects of plasmalogen synthesis, referred to as RCDP2 (GNPAT deficiency) and RCDP3 (AGPS deficiency). Furthermore, in all RCDP types, there is a direct correlation between phenotype severity and amounts of residual plasmalogens. Although most patients have the classical features described, milder phenotypes were reported [7]. These patients have RBC plasmalogen levels that are ~30% of the control mean and >2 standard deviations above the RCDP mean. Finally, patients with *PEX7* defects and near-normal RBC plasmalogen levels do not resemble RCDP at all, and instead manifest a phenotype similar to adult Refsum disease (ARD), secondary to phytanic acid accumulation over time [7]. Cerebellar degeneration, observed in long survivors with RCDP1 and in patients with ARD, might be related to accumulation of phytanic acid over time [3]. The loss of thiolase activity does not perturb very long chain fatty acid oxidation, because there is a second enzyme, Sterol Carrier Protein × (SCPx, EC 2.3.1.176), with thiolase activity.

1.2 Putative functions of plasmalogens

Although plasmalogen deficiency causes RCDP, the pathophysiology is unknown. This is partly because the normal functions of these compounds remain elusive. Plasmalogens are membrane glycerophospholipids distinguished by a fatty alcohol in vinyl-ether linkage at the sn-1 position. The alkyl-dihydroxyacetone phosphate formed in the peroxisome is reduced to alkyl-glycerophosphate by an acyl/akyl-DHAP reductase and further molecular modifications to form mature plasmalogens take place in the ER [8]. Here, the ether bond at sn-1 is reduced, and a polyunsaturated fatty acid, either arachidonic (AA) or docohexanoic acid (DHA) is preferentially placed at sn-2 [9]. The sn-3 position is modified to phosphatidyethanolamine or

[1]*Abbreviations used:* RCDP, Rhizomelic chondrodysplasia punctata; AGPS, alkyl-dihydroxyacetonephosphate synthase; PhyH, phytanoyl-CoA hydroxylase; ACAA1, 3-oxoacyl-CoA thiolase; AA, arachidonic acid; DHA, docohexanoic acid; PA, phytanic acid; PAS, Periodic acid-Schiff; LFB, Luxol fast blue

phosphatidylcholine. Plasmalogens constitute up to 20% of phospholipids in cell membranes and are more abundant in brain myelin, where they can account for 70% of the glycerophospholipid fraction, cardiac sarcolemna, neutrophils, monocytes and macrophages, and lowest in liver [8,10]. Seminolipid, a plasma membrane sulfo-galactosyl alkylglycerol, constitutes 90% of glycolipid in testes [11].

Plasmalogens are implicated in a number of structural functions of plasma membranes, as well as protein interactions and signaling functions. As intact molecules, they are prone to form non-lammellar lipid structures, suggesting that they perturb the membrane to facilitate fusion and fission events [12]. They are enriched in lipid raft microdomains (LRMs), distinct membrane regions involved in signal transduction and cell-cell interactions, and they are components of glycophosphatidylinositol (GPI) protein anchors [13]. In various experiments, plasmalogens were shown to selectively activate the cardiac muscle sodium-calcium exchanger, coupling excitation and contraction, and to regulate numbers of cell surface β-ardrenergic receptors [14,15]. Stimulation of phospholipase A2 results in selective hydrolysis of tissue plasmalogens to generate bioactive compounds AA, DHA and lysoplasmalogens [16]. In thyroid tissue, excess iodide reacts with the vinyl ether group of plasmalogens to release iodo-hexadecanal [17]. Similarly, chlorides generated by neutrophil myeloperoxidase release α-chloro fatty aldehydes from membrane plasmalogens [18]. Since the vinyl ether bond in plasmalogens is more susceptible to oxidation than their 1-acyl analogues, they might scavenge reactive oxygen species, thus ‘protecting’ other phospholipids and lipoproteins from oxidative damage. In fact, supplementation of plasmalogens to human endothelial cell cultures under hypoxic conditions mitigated the increase in reactive oxygen species observed in the untreated cells [19]. Plasmalogens are not always membrane bound, and are secreted into surfactant by type II pneumocytes, where they provide a unique reduction in both surface tension and viscosity [20]. Platelet Activating Factor (PAF) is a soluble alkyl-glycerophosphocholine that mediates inflammatory pathway signaling by binding to specific cell surface receptors. Plasmalogens are also somehow involved in intracellular cholesterol transport [21].

Although plasmalogen deficiency causes the primary pathology in RCDP, reduced amounts of these compounds have been detected in more common disorders. Several studies show plasmalogen depletion in brain tissues from patients with Alzheimer Disease and Down syndrome [22]. Reduced plasmalogens in tracheal aspirates from premature infants increase their risk for bronchopulmonary dysplasia [23]. Glycerophospholipids in the lens decrease with age, predisposing to senile cataract [24]. Plasmalogen depletion in these conditions could be secondary to oxidative damage, impairment of synthesis or stimulation of degradation. Nevertheless, the lower plasmalogen levels in these disorders might contribute to pathology and be preventable.

Most of the studies that have evaluated plasmalogen functions were done using in vitro systems. To further investigate the critical roles for plasmalogens in organ development and maintenance, and to explore therapy for plasmalogen deficient states, we generated a hypomorphic *Pex7* mouse model. Brites et al (2003) [25] generated a Pex7 null, and Rodemer et al (2003) [26] a GNPAT null mouse model, but these mice have reduced survival, limiting the investigations and therapeutic interventions that might be performed. The hypomorphic Pex7 mouse survives, is fertile and has a normal life span. However, they are smaller than their control littermates and develop early cataracts. Furthermore, they exhibit all the biochemical features of reduced Pex7 function, and therefore should prove useful for evaluating pathophysiology and treatment.

Materials and Methods

2.1 Construction of targeting cassette

Pex7 clones from a 129SVJ murine genomic library (Stratagene #946306) were identified using MmPex7 cDNA as probe [5]. A 5.5 kb XhoI-XhoI fragment containing exons 1–3 was cloned in pBS and fully sequenced. The neomycin cassette (neo^r) and PGK promoter from pGTNeo39 (New England Biolabs) was inserted in opposite orientation at the Afl2-Nhe1 site in intron 2. The final construct was linearized with NotI and electroporated into 129/SvEv ES cells. 400 neomycin resistant clones were screened by southern analysis and one correctly targeted clone identified. Chromosome number was normal and this was injected into C57BL/6 blastocysts. Chimeras were bred for germline transmission. C57BL/6 mice were purchased from Charles River Laboratories International, Inc., Wilmington, MA. Transgenic Core work was done at the Univ. of NY, Stonybrook. The Animal Care and Use Committees at Johns Hopkins and McGill University approved the mouse protocols.

2.2 Genotyping methods

For southern analysis, DNA was extracted from ES cells or tail tip, and 8–10 ug digested with EcoR1, electrophoresed overnight at 50V in 0.8% agaraose. Transfer to a nylon filter was performed (Turboblotter, GE Healthcare) using alkaline transfer buffer. Filters were UV cross-linked and hybridization was done overnight with Amersham Rapid-hyb buffer. Probes were ^{32}P labeled (Amersham Ready-To-Go DNA Labelling Beads, GE Healthcare). For PCR genotyping, gDNA was isolated from tail tips using Puregene (Qiagen), resuspended in 100 uL of Tris EDTA buffer and further diluted 1:4 for PCR. Primers for the wild type allele generate a 500 bp intron 2 fragment: 4106F 5′cagtcaacctctgtcaaagtc and 4091R 5′ gacatgctgacatcacctgc. Primers for the targeted allele generate a 600 bp fragment from neo^r to intron 2: 4021F 5′ctacttccatttgtcacgtcc and 4091R. We used 5 uL of gDNA, 200 mM dNTPs, 200 uM of each primer, Platinum™ Taq (Invitrogen) and 1X PCR buffer, TV 50 uL. PCR cycling was 98 × 2 min; 95 × 30s, 58 × 30s 72 × 36s for 39 cycles; 72 × 7 m.

2.3 Pex7 transcript evaluation

Total RNA was isolated from mouse tissues using TRIzol™ (Invitrogen). For northern analysis, we applied 15 ug per lane and electrophoresed 100V × 5h in formaldehyde gel and MOPS buffer. Hybridization was performed as per southern, using neutral transfer buffer and Mm*Pex7* cDNA as probe. Blots were re-probed with Hs*OAT* cDNA (84% identity to Mm*OAT*). For QPCR analysis, 5 ug total RNA was reverse transcribed using SuperScript ™ II (Invitrogen) and 10 pmol of poly-dT primer. For PCR, we used 5uL of first strand cDNA, primers 2277 F 5′ggcttatgcggccgagttc and 2276 R 5′cgtcgagaccctgtgacggt (Exons 1–3), or 2447F 5′ caggactacggcatcgc and 4R 5′ccacttgttgaacaacacaga (Exons 1–4), GAPDH control primers and iQ SYBR Green Supermix (BioRad Laboratories). Data was analyzed using relative gene expression ($2^{-\Delta\Delta CT}$ method) [27].

2.4 Cell cultures

Mouse embryonic fibroblasts were generated from E13.5 day embryos after evisceration, washing with PBS and mincing with a sterile razor in a 35 mm dish. 3 cc of trypsin was added per embryo, the tissue slurry transferred to a conical tube, cells disrupted by pipetting, disassociated cells transferred to media and the process repeated × 2. Lens epithelial cells were obtained by dissecting 10 lenses, incubating with 1.5 ml αMEM containing 25 mM HEPES/ NaOH(ph7.4) and 0.125% collagenase type CLS III at 37 °C × 30 m, gently disassociating tissue x15 m. Cells were pelleted at 300g × 5 m, washed and resuspended in α-MEM containing 20% FBS, and placed in culture dishes.

2.5 Evaluation of peroxisome functions

Plasmalogens, very long chain fatty acids and phytanic acid levels in tissues were obtained using standard methods in the Peroxisome Disease Laboratory at the Kennedy Krieger Institute [28,29]. Plasmalogen synthesis was performed using the double substrate, double isotope method of Roscher et al (1985) [30] to compare peroxisomal incorporation of ^{14}C-hexadecanol to microsomal incorporation of ^{3}H-hexadecyglycerol. Indirect immunofluorescence was performed on fibroblast cultures as reported [7]. For immunoblotting, tissue samples were homogenized and cells lysed, 30 ug of protein per lane was separated in 7.5% SDS-PAGE using Tris-Glycine-SDS running buffer. The proteins were electro-transferred to Hybond-P (Amersham Phamacia) in Tris-Glycine-Methanol transfer buffer. The membrane was blocked with 5% nonfat dry milk in TBS-Tween (0.1% Triton) overnight at 4 °C, then incubated with 1° antibody at room temperature × 1 h. Washing was done 5m × 6 in TBS-T. After incubation and washing with 2° HRP-antibody, ECL was performed (SuperSignal, Pierce).

2.5 Dietary supplements

Phytol (Sigma grade 97%) was solubilized in ether and added to mouse chow (Harlan Teklad 2018) to provide either 2.5 mg/gm or 5.0 mg/gm of chow; the ether was allowed to evaporate. Subsequently, we used an identical 0.5% phytol diet plus 1% soybean oil, prepared by Harlan-Teklad (Madison, WI). They also prepared the batyl alcohol (Sigma 99%) as 250 mg/kg of the same chow, to provide 50 mg/kg/day, based on an adult mouse consuming 4 gms of chow per day. Both dietary supplements were begun prior to mating and continued through life of the offspring. RBC plasmalogen levels reported for mice supplemented with batyl alcohol were obtained from mice backcrossed onto C57BL/6.

2.5 Mouse breeding and phenotyping

Mice were maintained as a stable inbred colony, segregating both C57BL/6 and 129/SvEv alleles. Breeding pairs were $Pex7^{neo/neo} \times Pex7^{neo/+}$ and heterozygote littermates were controls. We also maintained $Pex7^{neo/neo}$ and $Pex7^{+/+}$ colonies. Weights were obtained with a gm scale. Cataracts were evaluated using 0.5% midriacyl to dilate the pupil. Faxitron MX-20 Radiography System (Faxitron X-ray, Lincolnshire, IL) was used for skeletal x-rays. Autopsies were performed by the Phenotyping Core, Dept. of Comparative Medicine, Johns Hopkins Univ. Tissues were dissected and fixed in 10% buffered formalin or Bouin solution, paraffin embedded, decalcified, sectioned and stained with H&E, or Luxol fast blue, PAS and Cresyl violet for nerve sections.

Results

3.1 Generation of Pex7 hypomorphic mice

To obtain a murine model for RCDP1, and to avoid early lethality, we designed a hypomorphic Pex7 allele by inserting a neo^r cassette into intron 2, in reverse orientation to *Pex7* gene transcription. The use of cryptic splice sites in the neo^r cassette reduces the amount of wild type transcript produced, and placement in reverse orientation produces a more severe reduction in transcript [31,32]. The targeting construct, shown in Fig. 1A, was electroporated into 129/SvEv ES cells, and neomycin resistant clones were screened by southern analysis. A single clone containing a correctly targeted allele (see Fig. 1B) was injected into C57BL/6 blastocysts and chimeric offspring were bred to obtain $Pex7^{neo/+}$ germline heterozygotes; these were crossed to obtain $Pex7^{neo/neo}$ homozygotes. To evaluate *Pex7* transcript levels, we performed northern analysis and quantitative RT/PCR. *Pex7* was undetectable on northern analysis of total RNA from brain, liver, kidney and muscle (see Fig. 2). By quantitative RT/PCR we found 3.2±3.6% of wild type *Pex7* transcript in brain (n=4), 0.064±0.02% in liver

(n=4), 1.9±0.2% in kidney (n=4), lung 1.8±1.1% (n=8). $Pex7^{neo+/+}$ transcript levels were between 10–50% of wild type in these tissues.

3.2 Phenotype of $Pex7^{neo/neo}$ mice

The $Pex7^{neo/neo}$ mice are born in expected ratios from $Pex7^{neo/+}$ parents, are fertile and have a normal life span. However, they are around 70–80% ($p < 0.004$) as large in size and weight compared to their heterozygote littermates (Fig. 3). This difference is present from birth and through the monitoring periods, indicating that growth retardation begins prenatally. X-ray analysis showed a smaller skeleton at 3 mos in the $Pex7^{neo/neo}$ mice compared to their control littermates, but no obvious skeletal abnormalities. All $Pex7^{neo/neo}$ mice had visible cataracts by 2–6 wks of age. Diffuse haziness of the lens was appreciated before the full opacity presented. In contrast, none of the $Pex7^{neo/+}$ or $Pex7^{+/+}$ mice developed cataracts in the first yr of life. These phenotypes are illustrated in Fig. 3. Heterozygote phenotypes did not vary substantially from wild type.

3.3 Peroxisome functions

Tissue plasmalogen levels in $Pex7^{neo/neo}$ mice, reported as % total fatty acids, varied from around 50% in RBCs, to around 30% of their littermate controls in brain, heart and lens epithelial cells (Table 1). DHA levels in RBCs from $Pex7^{neo/neo}$ mice were around 66% of $Pex7^{neo/+}$controls. Plasmalogen biosynthesis, a measure of both GNPAT and AGPS enzyme activities, and PA oxidation was reduced in $Pex7^{neo/neo}$ embryonic fibroblasts compared to littermate controls. PA levels were minimal in all mice, as expected, since this compound is exclusively dietary in origin and is absent from mouse chow. To directly evaluate peroxisomal import of PTS2 targeted proteins, we examined embryonic fibroblast cultures by indirect immunofluorescence and confirmed reduced import of thiolase and AGPS (Fig. 4). Whole cell lysates, processed by immunoblotting, showed reduced amounts of processed (mature) thiolase and AGPS, corresponding to the inability to import PTS2-targeted proteins into peroxisomes (Fig. 5). Although antiserum is not available to evaluate endogenous Pex7 protein levels, the accumulated data indicate significant reduction in Pex7 peroxin in $Pex7^{neo/neo}$ mice.

3.3 Lens and skeletal evaluations

Autopsies were performed on two $Pex7^{neo/neo}$ adult males and compared to a $Pex7^{neo/+}$ control. Lens sections (Fig. 6, A–D) showed posterior proliferation of epithelial cells and dramatic ballooning of lens fiber cells, resulting in retained nuclei and abnormal layering of lens fibers throughout the lens. The lens capsule is thickened. Normally, as in the control, the epithelium extends from the anterior pole to the equator; there is no posterior cell layer and no nuclei remain in the central lens. Other tissues were similar to controls when evaluated by H & E stain. At day one of life, we observed delay in ossification centers of the foot in the $Pex7^{neo/neo}$ mice (Fig. 6, E–F).

3.3 Tissue accumulation of phytanic acid upon dietary phytol supplementation

In order to determine whether the $Pex7^{neo/neo}$ mice could accumulate PA (3R,S,7R,11R,15-tetramethylhexadecanoic acid) due to their PhyH defects, similar to RCDP and ARD patients, we added 0.5% (5 mg/gm) phytol to mouse chow and followed mice on continuous supplementation, begun at conception. In ARD patients, plasma PA levels are usually >200 uM, and can be >1000 uM at diagnosis; PA can account for 5–30% of fatty acids in plasma and up to 50% in the liver [33]. Plasma and tissue PA levels in 3–5 month $Pex7^{neo/neo}$ old mice were similar to that observed in ARD (Table 2). There was no substantial increase in pristanic acid (2,6,10,14 tetramethylpentadecanoic acid), indicating that the pathway is blocked at PhyH.

Since PA is an endogenous ligand for the transcription factor PPARα, elevated levels should result in the increased expression of genes encoding enzymes involved in fatty acid catabolism [34]. Consistent with the stimulation of PPARα related gene expression, we noted decreased plasma total saturated fatty acid levels in the $Pex7^{neo/neo}$ mice on phytol supplementation, as compared to $Pex7^{neo/+}$ mice (Table 2). Poor weight gain was obvious after weaning and, at 6 wks of age, there was a 15–20% weight decrease in the $Pex7^{neo/neo}$ mice on phytol compared to those not receiving phytol, but only a 5% weight loss in the $Pex7^{neo/+}$ on phytol (n=14). There were smaller, fewer litters in the $Pex7^{neo/neo}$ mice on phytol supplementation. Several $Pex7^{neo/neo}$ mice died, but no $Pex7^{neo/+}$ mice, and they were noted to lose weight for several days prior to death. To evaluate chronic effects of PA accumulation, autopsy was performed on a $Pex7^{neo/neo}$ female at 15 mos and a $Pex7^{neo/+}$ male mouse at 13 mos of age. Plasma PA levels prior to euthanasia were 1234 and 127 uM, respectively. Vacuolation, consistent with lipid deposits, was observed in multiple tissues including liver, heart and adrenal glands, and was more severe in the homozygote. In the $Pex7^{neo/neo}$ mouse, the liver was enlarged and nodular with hepatocyte vacuolation and degenerative changes, portal and periportal aggregates of vacuolated macrophages and inflammatory infiltrates (Fig. 7A, B). Although additional mice need to be evaluated, the liver histopathology is consistent with that reported from other mouse models supplemented with phytanic acid (see discussion). Peripheral nerve demyelination is a classic feature of adult Refsum disease. In the cauda equina, we observed focal demyelination of a spinal rootlet, which was not seen in the $Pex7^{neo/+}$ mouse (Fig 7C, D). Although intraneural PAS/LFB positive deposits in the hippocampus is expected in C57Bl6 mice older than 6 mos of age, they appeared more prominent in the $Pex7^{neo/neo}$ compared to the $Pex7^{neo/+}$ mouse (Fig 7, E–F).

3.4 Dietary batyl alcohol supplementation as therapy

Batyl alcohol (1-*O*-octadecyl-*sn*-glycerol) is a C18:0 ether-substituted glycerol molecule. Since batyl alcohol already contains an ether bond, it can serve as a precursor in the biosynthesis of plasmalogens and bypass the peroxisomal step in the synthesis of these compounds. It was shown that batyl alcohol, when fed to rodents, was directly utilized to synthesize plasmalogens in most tissues, although there was low incorporation into brain [35]. To determine if batyl alcohol improves plasmalogen levels and phenotype in our $Pex7^{neo/neo}$ mice, we began 50 mg/kg/day supplementation prior to birth in a cohort of $Pex7^{neo/neo}$ and $Pex7^{neo/+}$ mice (n=12). We found no differences in body weight and cataract phenotype between the treated and untreated mice. RBC plasmalogens were measured after 2 mos of treatment (n=2). The results, reported in Table 3, show partial recovery of plasmalogen species in the $Pex7^{neo/neo}$ mouse on treatment. In addition, we noted an increase in absolute levels of C16 and C18 fatty acids, as well as DHA.

Discussion

We have shown that a *Pex7* hypomorphic model expressing < 5% of *Pex7* transcript in various tissues has moderate defects in plasmalogen synthesis. This profile mimics the milder RCDP1 patient phenotypes, and highlights prior observations that plasmalogen deficiency determines disease severity. An ARD patient previously reported with a splice site mutation in *PEX7*, produced small amounts of wild type *PEX7* transcript, and this was thought to be responsible for the milder phenotype [7]. Both *Pex7* and *GNPAT* null mouse models were previously reported and these show reduced survival, sterility and neurological abnormalities [25,26]. Although we did not perform neurological evaluations in our in $Pex7^{neo/neo}$ mice, their unstressed clinical examination did not suggest any gross defects. Taken together, both the mouse and human data suggest that small increases in *Pex7* transcript can ameliorate the phenotype, which should greatly facilitate any practical aspects of treatment.

In the hypomorphic *Pex7* model, the skeleton and lens are the most sensitive markers for plasmalogen deficiency. Ossification delay was also reported in *Pex7* null mice [25] and is likely related to the growth failure observed in both mice and human patients [37]. A subtle rhizomelia was observed, but not measured, in the *GNPAT* null mice [26]. Chondrodysplasia punctata (CDP) was not observed in either model, and may not occur due to differences in murine physiology. CDP is also a feature of sterol Δ8-isomerase deficiency (CDPX2), and likewise, is not reproduced in the murine model [38]. CDP also occurs in Keutel syndrome due to defects in Matrix GLA protein. Mice deficient in matrix GLA protein develop inappropriate calcification of growth plate cartilage as adults, with calcification extending into the zone of proliferating chondrocytes resulting in disorganized chondrocyte columns [39]. In contrast, the few reports of bone histology in RCDP patients show primary degeneration of resting zone chondrocytes and cartilage matrix, with foci of calcification throughout the epiphyses [40]. Cataracts were studied in the GNPAT null mouse and the description was similar to our hypomorphic Pex7 model, although additional extra-lenticular findings were described in the former [26].

We found low DHA levels in out Pex7 hypomorphic mice. DHA is preferentially stored at the sn-2 position in plasmalogens, and, in CHO cell models, when plasmalogens are low DHA levels can also be low [41]. However, this has not been systematically studied in RCDP. DHA levels were reduced in the GNPAT null mouse brain, but were not reported in the Pex7 null mouse. In the Pex7 null model, Brites et al (2003) [24] report that elevation of VLCFAs, including C26:0/C22:0 ratios, were 2–3 x control values at P0.5 but this difference resolved in adulthood. They proposed that ACAA1 thiolase plays a more functional role in B-oxidation prenatally. We found no significant differences between C26:0/C22:0 ratios in brain tissues (n=8) from $Pex7^{neo/neo}$ and $Pex7^{+/+}$ mice at P3.0 (data not shown).

There is abundant literature on phytol feeding of wild type mice strains, as well as mice with targeted alleles in the branched chain fatty acid pathways: Pex7, PhyH, AMACR, and ScPx. (25, 42–44). Wild type C57BL/6 females can show more extensive liver pathology than males, due to their relative decreased expression of SCPx [44]. Overall, 0.25–1.0 % phytol supplementation causes weight loss with normal food intake, suggesting an effect on metabolism. Once metabolized to PA, a natural PPARα ligand, there is induction of genes encoding enzymes of fatty acid oxidation in peroxisomes and mitochondria, peroxisome proliferation, hepatomegaly and liver necrosis. Clofibrate, a well-described PPARα ligand, causes heptocarcinogenesis when administered to rodents. In contrast, hepatotoxicity associated with PPARα induction is not observed in humans. This differential outcome might be caused by suppression of the microRNA let-7c gene by murine PPARα, which upregulates c-myc, resulting in enhanced hepatocellular proliferation [45]. Studying the pathophysiology of PA accumulation without developing hepatic toxicity could be accomplished using PPARα humanized mice, which were shown to be resistant to these toxic effects [45].

There are several possible reasons why batyl alcohol supplementation did not abort the lens or skeletal phenotype in the $Pex7^{neo/neo}$ mice. These tissues could be more refractory to plasmalogen rescue because they are relatively avascular, and might need higher doses. A prior study in rats has shown that batyl alcohol does not cross the placenta, but was transferred into the mother's milk [35]. Thus, the developmental timing of these defects, and whether or not these drugs cross the placenta and the blood-brain barrier will be important to determine, especially as the RCDP phenotype starts prenatally. Several studies have shown that supplementation with natural alkylglycerols results in their incorporation into plasmalogens in multiple tissues, without any apparent toxic effects, in rodents and several patients with Zellweger spectrum disorder [35,46,47]. Thus, this is an important possible therapy that can now be directly assessed with this model. In this report, we observed an increase in C16:0, C18:0 and C18:1 fatty acids in RBC membranes after batyl alcohol treatment. We suggest the

increase in these fatty acids derives from cleavage of the ether bond in batyl alcohol, and the C18:0 aldehyde is subsequently oxidized to fatty acid. The enzymatic cleavage of the ether-linked chain of alkylglycerol releasing a fatty aldehyde has been demonstrated [36]. If a major portion of the batyl alcohol is not converted to plasmalogen lipid, this could be further studied to determine drug modifications that enhance conversion or tissue delivery. Alternatively, the observed increase in fatty acids could reflect an induction of synthesis or the overall recovery of other lipids in RBC membranes. In fact, we also observed a recovery in DHA levels after batyl alcohol treatment.

Plasmalogen levels are reduced in a number of more common neurodegenerative disorders, but neither the mechanism nor significance of these findings is known. Some of the most consistent evidence for plasmalogen depletion is from brain tissue in patients with Alzheimer disease [22,48]. PAS positive intraneural deposits, immunoreactive for Tau protein and α-synuclein, were described in C57BL/6 mice [49]. Although not identical to the plaque lesions of Alzheimer disease, they represent a neurodegenerative process that might share pathogenic mechanisms. The finding of increased PAS positive intraneural deposits in the older Pex7 hypormophic mouse relative to the heterozygote can be further investigated to determine whether they are related to the plasmalogen deficiency or to the phytol supplementation, and whether they contain Tau protein. It is also possible that sex and age differences underlie these findings.

Extended work done on the GNPAT null mouse shows that plasmalogens are enriched in lipid raft domains [26] and clarifies specific roles for these compounds in myelination and Purkinje cell innervation [50], as well as a functional blood-testis barrier [51]. Heterozygotes for the *Pex7* null allele were crossed to ABCD1 (encoding the X-linked adrenoleukodystrophy protein, ALDP) null mice to generate double null mutants. In those that survived past weaning, it could be shown that plasmalogens protect nerve cells from damage caused by VLCFA accumulation [52]. Thus roles for plasmalogens in human health and disease are beginning to yield to investigation, and the Pex7 hypomorphic model has its niche in evaluating phenotype progression, especially in the lens and bone, and to test potential therapies.

Acknowledgments

This project was funded by an NIH R01HD39747 from the NICHD to Johns Hopkins University (NB). We also acknowledge the support of the Nicholas Davis Duke Memorial Endowment Fund at the Johns Hopkins Dept. of Pediatrics, Dr. Cory Brayton, Director of the Phenotyping Core at Johns Hopkins for review of the histopathology, Drs. Debasish Sinha and Sam Zigler, of the Wilmer Eye Institute, Johns Hopkins, for review of the lens histology.

References

1. White AL, Modaff P, Holland-Morris F, Pauli RM. Natural history of rhizomelic chondrodysplasia punctata. American Journal of Medical Genetics 2003;118A:332–342. [PubMed: 12687664]
2. Steinberg SJ, Dodt G, Raymond GV, Braverman NE, Moser AB, Moser HW. Peroxisome biogenesis disorders. Biochimica et Biophysica Acta 2006;1763:1733–1748. [PubMed: 17055079]
3. Powers JM, Kenjarski TP, Moser AB, Moser HW. Cerebellar atrophy in chronic rhizomelic chondrodysplasia punctata: a potential role for phytanic acid and calcium in the death of its Purkinje cells. Acta Neuropathol (Berl) 1999;98:129–134. [PubMed: 10442551]
4. Bams-Mengerink AM, Majoie CB, Duran M, Wanders RJ, Van Hove J, Scheurer CD, Barth PG, Poll-The BT. MRI of the brain and cervical spinal cord in rhizomelic chondrodysplasia punctata. Neurology 2006;66:798–803. discussion 789. [PubMed: 16567694]
5. Braverman N, Steel G, Obie C, Moser A, Moser H, Gould SJ, Valle D. Human PEX7 encodes the peroxisomal PTS2 receptor and is responsible for rhizomelic chondrodysplasia punctata. Nat Genet 1997;15:369–376. [PubMed: 9090381]

6. Wanders RJ, Waterham HR. Biochemistry of mammalian peroxisomes revisited. Annual Review of Biochemistry 2006;75:295–332.
7. Braverman N, Chen L, Lin P, Obie C, Steel G, Douglas P, Chakraborty PK, Clarke JT, Boneh A, Moser A, Moser H, Valle D. Mutation analysis of PEX7 in 60 probands with rhizomelic chondrodysplasia punctata and functional correlations of genotype with phenotype. Hum Mutat 2002;20:284–297. [PubMed: 12325024]
8. Nagan N, Zoeller RA. Plasmalogens: biosynthesis and functions. Prog Lipid Res 2001;40:199–229. [PubMed: 11275267]
9. Brites P, Waterham HR, Wanders RJ. Functions and biosynthesis of plasmalogens in health and disease. Biochimica et Biophysica Acta 2004;1636:219–231. [PubMed: 15164770]
10. Rapport MM, Lerner B. The structure of plsmalogens. IV. Lipids in normal and neoplastic tissues of man and in normal tissues of rabbit and rat. Biochimica et Biophysica Acta 1959;33:319–325. [PubMed: 13670900]
11. Zhang Y, Hayashi Y, Cheng X, Watanabe T, Wang X, Taniguchi N, Honke K. Testis-specific sulfoglycolipid, seminolipid, is essential for germ cell function in spermatogenesis. Glycobiology 2005;15:649–654. [PubMed: 15659616]
12. Lohner K. Is the high propensity of ethanolamine plasmalogens to form non-lamellar lipid structures manifested in the properties of biomembranes? Chem Phys Lipids 1996;81:167–184. [PubMed: 8810047]
13. Pike LJ, Han X, Chung KN, Gross RW. Lipid rafts are enriched in arachidonic acid and plasmenylethanolamine and their composition is independent of caveolin-1 expression: a quantitative electrospray ionization/mass spectrometric analysis. Biochemistry 2002;41:2075–2088. [PubMed: 11827555]
14. Hale CC, Ebeling EG, Hsu FF, Ford DA. The selective activation of the cardiac sarcolemmal sodium-calcium exchanger by plasmalogenic phosphatidic acid produced by phospholipase D. FEBS Lett 1998;422:247–251. [PubMed: 9490017]
15. Styger R, Wiesmann UN, Honegger UE. Plasmalogen content and beta-adrenoceptor signalling in fibroblasts from patients with Zellweger syndrome. Effects of hexadecylglycerol. Biochimica et Biophysica Acta 2002;1585:39–43. [PubMed: 12457713]
16. Meyer MC, Rastogi P, Beckett CS, McHowat J. Phospholipase A2 inhibitors as potential anti-inflammatory agents. Curr Pharm Des 2005;11:1301–1312. [PubMed: 15853686]
17. Panneels V, Macours P, Van den Bergen H, Braekman JC, Van Sande J, Boeynaems JM. Biosynthesis and metabolism of 2-iodohexadecanal in cultured dog thyroid cells. J Biol Chem 1996;271:23006–23014. [PubMed: 8798488]
18. Skaff O, Pattison DI, Davies MJ. The vinyl ether linkages of plasmalogens are favored targets for myeloperoxidase-derived oxidants: a kinetic study. Biochemistry 2008;47:8237–8245. [PubMed: 18605737]
19. Zoeller RA, Grazia TJ, LaCamera P, Park J, Gaposchkin DP, Farber HW. Increasing plasmalogen levels protects human endothelial cells during hypoxia. Am J Physiol Heart Circ Physiol 2002;283:H671–679. [PubMed: 12124215]
20. Rudiger M, Tolle A, Meier W, Rustow B. Naturally derived commercial surfactants differ in composition of surfactant lipids and in surface viscosity. Am J Physiol Lung Cell Mol Physiol 2005;288:L379–383. [PubMed: 15501950]
21. Munn NJ, Arnio E, Liu D, Zoeller RA, Liscum L. Deficiency in ethanolamine plasmalogen leads to altered cholesterol transport. J Lipid Res 2003;44:182–192. [PubMed: 12518037]
22. Hartmann T, Kuchenbecker J, Grimm MO. Alzheimer's disease: the lipid connection. J Neurochem 2007;103(Suppl 1):159–170. [PubMed: 17986151]
23. Rudiger M, von Baehr A, Haupt R, Wauer RR, Rustow B. Preterm infants with high polyunsaturated fatty acid and plasmalogen content in tracheal aspirates develop bronchopulmonary dysplasia less often. Crit Care Med 2000;28:1572–1577. [PubMed: 10834714]
24. Huang L, Grami V, Marrero Y, Tang D, Yappert MC, Rasi V, Borchman D. Human lens phospholipid changes with age and cataract. Invest Ophthalmol Vis Sci 2005;46:1682–1689. [PubMed: 15851569]
25. Brites P, Motley AM, Gressens P, Mooyer PA, Ploegaert I, Everts V, Evrard P, Carmeliet P, Dewerchin M, Schoonjans L, Duran M, Waterham HR, Wanders RJ, Baes M. Impaired neuronal

migration and endochondral ossification in Pex7 knockout mice: a model for rhizomelic chondrodysplasia punctata. Human Molecular Genetics 2003;12:2255–2267. [PubMed: 12915479]

26. Rodemer C, Thai TP, Brugger B, Kaercher T, Werner H, Nave KA, Wieland F, Gorgas K, Just WW. Inactivation of ether lipid biosynthesis causes male infertility, defects in eye development and optic nerve hypoplasia in mice. Human Molecular Genetics 2003;12:1881–1895. [PubMed: 12874108]
27. Livak KJ, Schmittgen TD. Analysis of relative gene expression data using real-time quantitative PCR and the 2(-Delta Delta C(T)) Method. Methods 2001;25:402–408. [PubMed: 11846609]
28. Dacremont G, Cocquyt G, Vincent G. Measurement of very long-chain fatty acids, phytanic and pristanic acid in plasma and cultured fibroblasts by gas chromatography. J Inherit Metab Dis 1995;18 (Suppl 1):76–83. [PubMed: 9053557]
29. Dacremont G, Vincent G. Assay of plasmalogens and polyunsaturated fatty acids (PUFA) in erythrocytes and fibroblasts. J Inherit Metab Dis 1995;18(Suppl 1):84–89. [PubMed: 9053558]
30. Roscher A, Molzer B, Bernheimer H, Stockler S, Mutz I, Paltauf F. The cerebrohepatorenal (Zellweger) syndrome: an improved method for the biochemical diagnosis and its potential value for prenatal detection. Pediatr Res 1985;19:930–933. [PubMed: 4047762]
31. Meyers EN, Lewandoski M, Martin GR. An Fgf8 mutant allelic series generated by Cre- and Flp-mediated recombination. Nat Genet 1998;18:136–141. [PubMed: 9462741]
32. Nagy A, Moens C, Ivanyi E, Pawling J, Gertsenstein M, Hadjantonakis AK, Pirity M, Rossant J. Dissecting the role of N-myc in development using a single targeting vector to generate a series of alleles. Curr Biol 1998;8:661–664. [PubMed: 9635194]
33. Horn MA, van den Brink DM, Wanders RJ, Duran M, Poll-The BT, Tallaksen CM, Stokke OH, Moser H, Skjeldal OH. Phenotype of adult Refsum disease due to a defect in peroxin 7. Neurology 2007;68:698–700. [PubMed: 17325280]
34. Ellinghaus P, Wolfrum C, Assmann G, Spener F, Seedorf U. Phytanic acid activates the peroxisome proliferator-activated receptor alpha (PPARalpha) in sterol carrier protein 2-/ sterol carrier protein x-deficient mice. J Biol Chem 1999;274:2766–2772. [PubMed: 9915808]
35. Das AK, Holmes RD, Wilson GN, Hajra AK. Dietary ether lipid incorporation into tissue plasmalogens of humans and rodents. Lipids 1992;27:401–405. [PubMed: 1630273]
36. Rizzo WB, Heinz E, Simon M, Craft DA. Microsomal fatty aldehyde dehydrogenase catalyzes the oxidation of aliphatic aldehyde derived from ether glycerolipid catabolism: implications for Sjogren-Larsson syndrome. Biochimica et Biophysica Acta 2000;1535:1–9. [PubMed: 11113626]
37. Theander G, Pettersson H. Calcification in chondrodysplasia punctata. Relation to ossification and skeletal growth. Acta Radiol Diagn (Stockh) 1978;19:205–222. [PubMed: 654946]
38. Derry JM, Gormally E, Means GD, Zhao W, Meindl A, Kelley RI, Boyd Y, Herman GE. Mutations in a delta 8-delta 7 sterol isomerase in the tattered mouse and X-linked dominant chondrodysplasia punctata. Nat Genet 1999;22:286–290. [PubMed: 10391218]
39. Luo G, Ducy P, McKee MD, Pinero GJ, Loyer E, Behringer RR, Karsenty G. Spontaneous calcification of arteries and cartilage in mice lacking matrix GLA protein. Nature 1997;386:78–81. [PubMed: 9052783]
40. Poulos A, Sheffield L, Sharp P, Sherwood G, Johnson D, Beckman K, Fellenberg AJ, Wraith JE, Chow CW, Usher S, et al. Rhizomelic chondrodysplasia punctata: clinical, pathologic, and biochemical findings in two patients. The Journal of Pediatrics 1988;113:685–690. [PubMed: 3171792]
41. Gaposchkin DP, Zoeller RA. Plasmalogen status influences docosahexaenoic acid levels in a macrophage cell line. Insights using ether lipid-deficient variants. J Lipid Res 1999;40:495–503. [PubMed: 10064738]
42. Ferdinandusse S, Zomer AW, Komen JC, van den Brink CE, Thanos M, Hamers FP, Wanders RJ, van der Saag PT, Poll-The BT, Brites P. Ataxia with loss of Purkinje cells in a mouse model for Refsum disease. Proc Natl Acad Sci U S A 2008;105:17712–17717. [PubMed: 19004801]
43. Savolainen K, Kotti TJ, Schmitz W, Savolainen TI, Sormunen RT, Ilves M, Vainio SJ, Conzelmann E, Hiltunen JK. A mouse model for alpha-methylacyl-CoA racemase deficiency: adjustment of bile acid synthesis and intolerance to dietary methyl-branched lipids. Human Molecular Genetics 2004;13:955–965. [PubMed: 15016763]

44. Mackie JT, Atshaves BP, Payne HR, McIntosh AL, Schroeder F, Kier AB. Phytol-induced hepatotoxicity in mice. Toxicol Pathol 2009;37:201–208. [PubMed: 19188468] Farooqui AA, Ong WY, Horrocks LA. Plasmalogens, docosahexaenoic acid and neurological disorders. Adv Exp Med Biol 2003;544:335–354. [PubMed: 14713251]

45. Gonzalez FJ, Shah YM. PPARalpha: mechanism of species differences and hepatocarcinogenesis of peroxisome proliferators. Toxicology 2008;246:2–8. [PubMed: 18006136]

46. Wilson GN, Holmes RG, Custer J, Lipkowitz JL, Stover J, Datta N, Hajra A. Zellweger syndrome: diagnostic assays, syndrome delineation, and potential therapy. Am J Med Genet 1986;24:69–82. [PubMed: 3706414]

47. Blank ML, Cress EA, Smith ZL, Snyder F. Dietary supplementation with ether-linked lipids and tissue lipid composition. Lipids 1991;26:166–169. [PubMed: 2051899]

48. Farooqui AA, Ong WY, Horrocks LA. Plasmalogens, docosahexaenoic acid and neurological disorders. Adv Exp Med Biol 2003;544:335–354. [PubMed: 14713251]

49. Krass KL, Colinayo V, Ghazalpour A, Vinters HV, Lusis AJ, Drake TA. Genetic loci contributing to age-related hippocampal lesions in mice. Neurobiol Dis 2003;13:102–108. [PubMed: 12828934]

50. Teigler A, Komljenovic D, Draguhn A, Gorgas K, Just WW. Defects in myelination, paranode organization and Purkinje cell innervation in the ether lipid-deficient mouse cerebellum. Human Molecular Genetics 2009;18:1897–1908. [PubMed: 19270340]

51. Komljenovic D, Sandhoff R, Teigler A, Heid H, Just WW, Gorgas K. Disruption of blood-testis barrier dynamics in ether-lipid-deficient mice. Cell Tissue Res 2009;337:281–299. [PubMed: 19495798]

52. Brites P, Mooyer PA, El Mrabet L, Waterham HR, Wanders RJ. Plasmalogens participate in very-long-chain fatty acid-induced pathology. Brain 2009;132:482–492. [PubMed: 19022859]

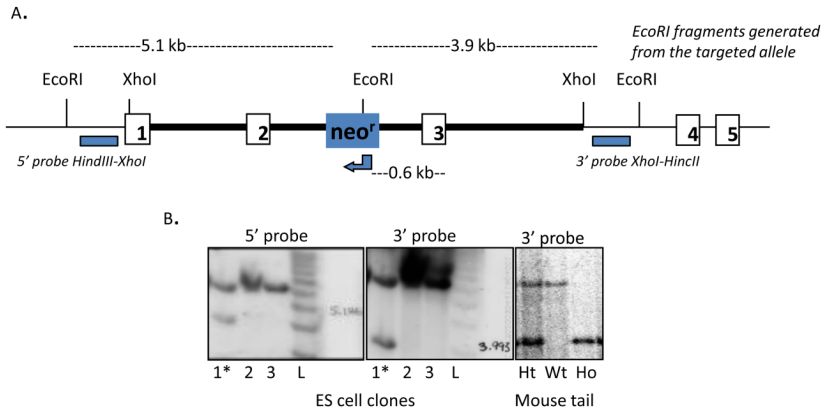

Fig. 1.

(A) Diagram of Xho1-Xho1 targeting construct, containing Pex7 exons 1–3, and genomic sequence flanking the targeting construct. Neo^r is inserted at AflII-NheI sites, removing 10 bps of intron 2. EcoR1 sites and probes used for the diagnostic southern digests are shown. (B) ES clone 1 shows correct position of the targeting construct by southern analysis. On the left, the 5′probe detects a 5.1 kb fragment; center, 3′ probe detects a 3.9 kb fragment. Right, both probes detect the correct fragment in tail gDNA, verifying germline transmission (only 3′ probe is shown). L, ladder.

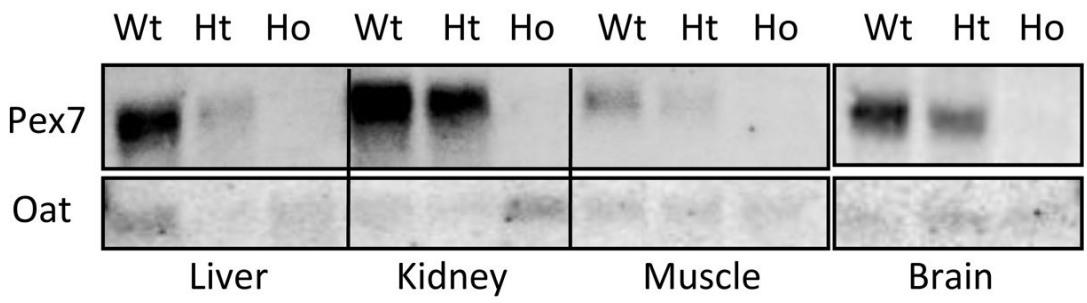

Fig. 2.

Northern analysis shows reduced levels of Pex7 transcript in the Pex7 $^{neo/neo}$ homozygotes (Ho) compared to Pex7 $^{neo/+}$ heterozygote (Ht) and Pex7 $^{+/+}$ wild type (Wt) littermate controls. Although RNA loading was not equivalent for the liver and kidney samples, it is clear that amounts of Pex7 in the Ho are negligible.

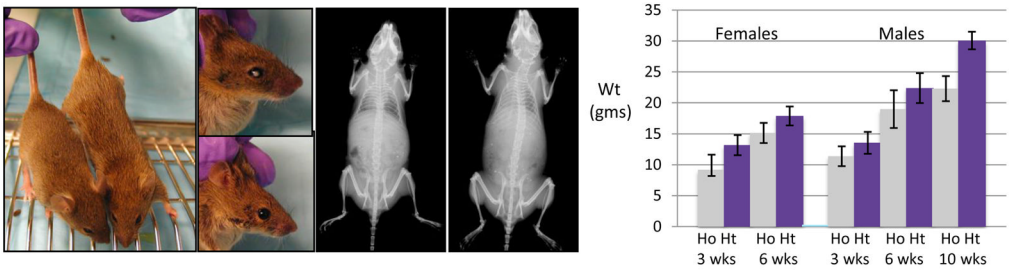

Fig. 3.

Top left, male littermates at 2 mo, Pex7$^{neo/neo}$ (left) compared to Pex7$^{neo/+}$ (right). Top center, dilated pupil outlines cataract in same Pex7$^{neo/neo}$ male. Next, x-rays of male littermates at 3 mo, Pex7$^{neo/neo}$ (left) compared to Pex7$^{neo/+}$ (right). Note smaller skeleton of Pex7$^{neo/neo}$ mice. Right, mean weight and std deviation plotted for 12 Pex7$^{neo/neo}$ (Ho) and 12 Pex7$^{neo/+}$ (Ht) females and males at 3, 6 and 10 wks of age. Weights for Pex7$^{neo/+}$ and Pex7$^{+/+}$ mice were similar.

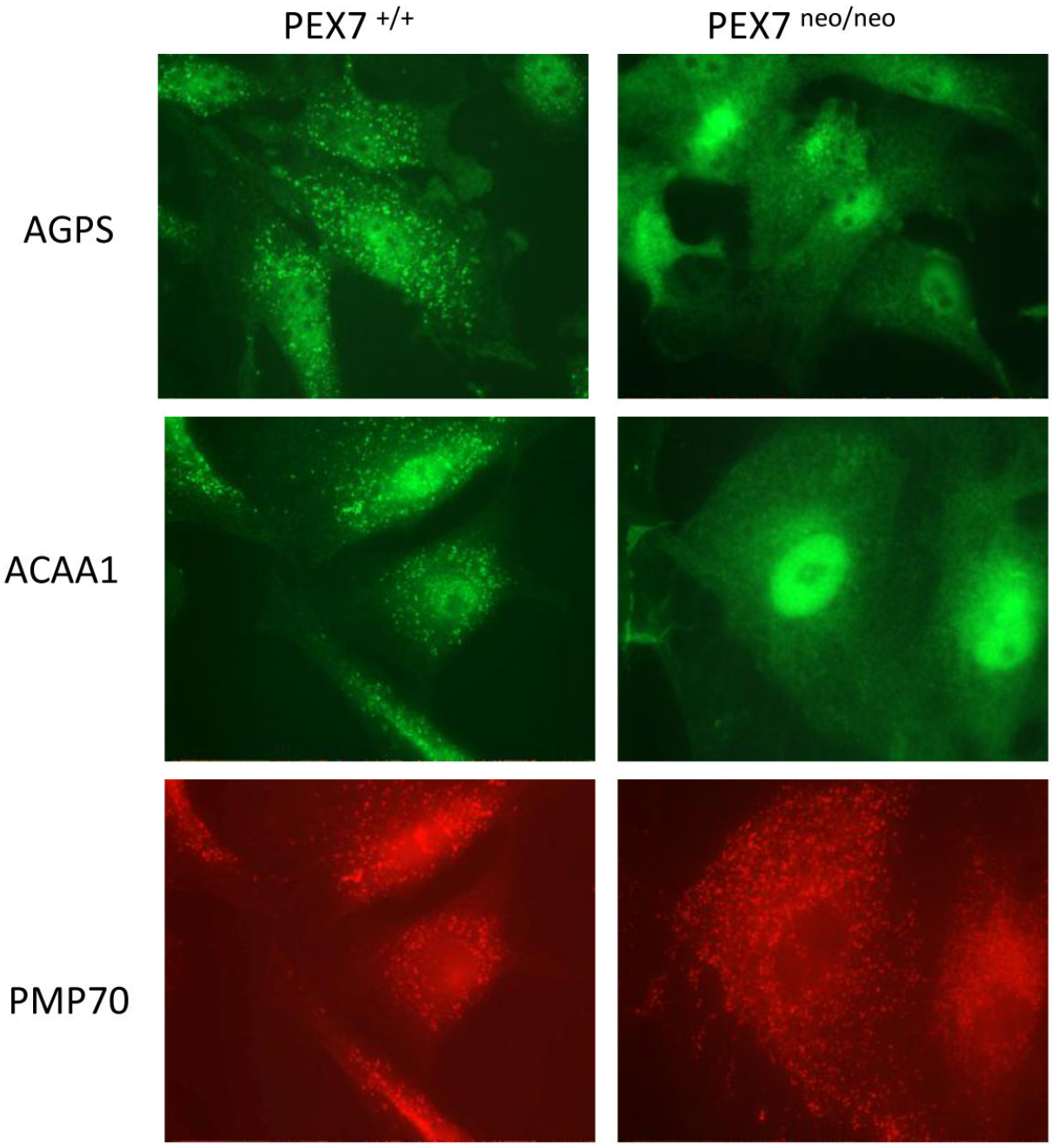

Fig. 4.

Reduced peroxisome import of PTS2-targeted matrix proteins, AGPS and thiolase, in the Pex7$^{neo/neo}$ cells visualized by indirect immunofluorescence. Embryonic fibroblasts were fixed, permeabilized and stained with AGPS antiserum, top panel, and thiolase, middle panel. There is robust import of AGPS and thiolase in the control cell lines, but this is reduced in the Pex7$^{neo/neo}$ cells. Co-localization of thiolase and the peroxisome marker, PMP70, bottom panel, shows that peroxisomes are present in usual amounts in both Pex7$^{+/+}$ and Pex7$^{neo/neo}$ cell lines

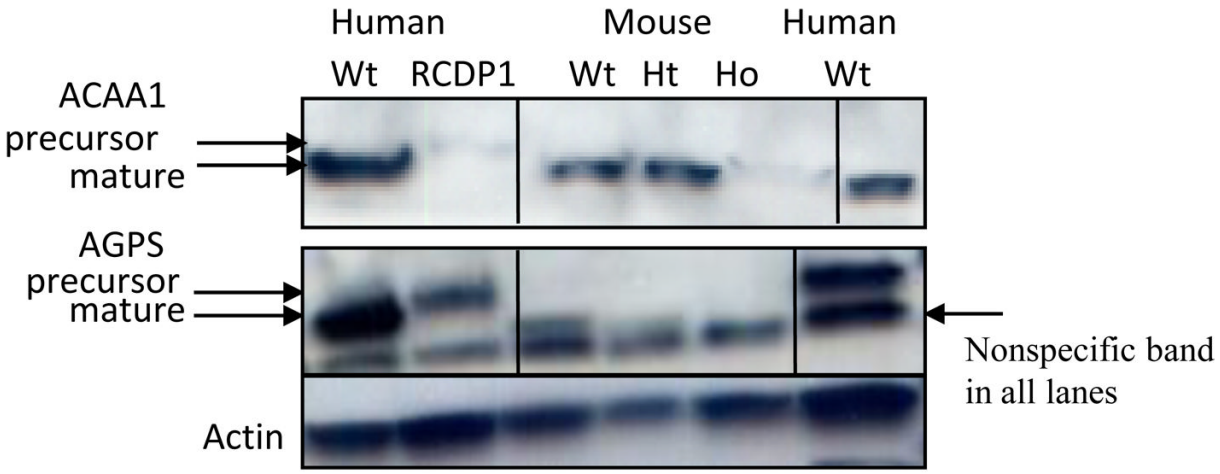

Fig. 5.

Amounts of ACAA1 and AGPS in human and corresponding mouse embryonic fibroblasts. Immunoblots were made from whole cell lysates, and filters were hybridized with ACAA1 or AGPS antiserum. The N-terminus of PTS2 targeted matrix proteins is removed inside the peroxisome to generate the smaller, mature protein. Loss of Pex7 targeting results in a cytosolic precursor protein that is unstable and degraded.

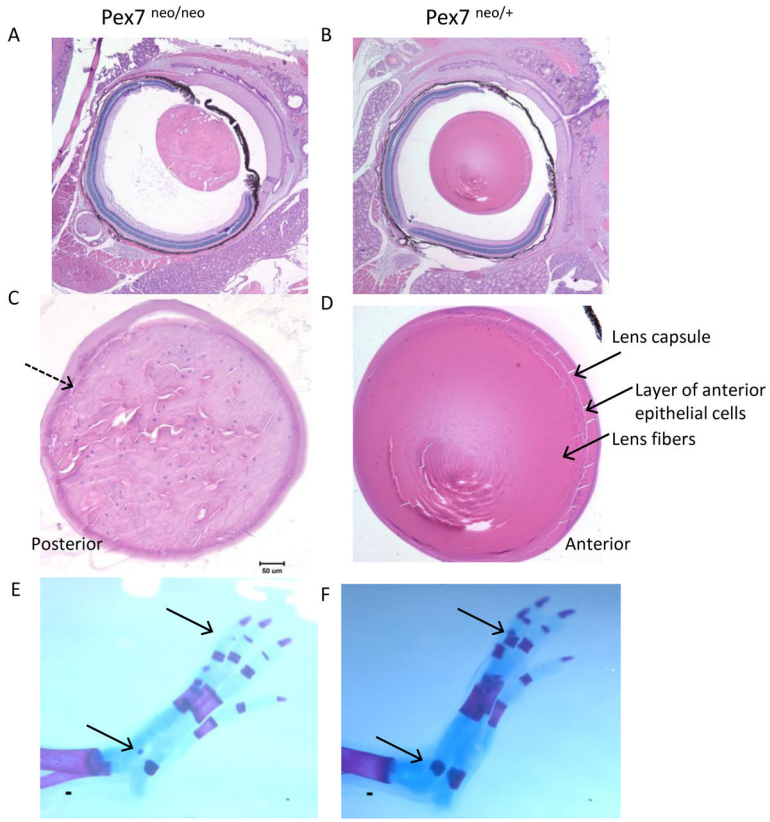

Fig. 6.

(A, B) H & E stain at 2 mos shows normal ocular structures, except for the lens. (C, D) Lens cross sections show a thickened capsule, posterior proliferation of epithelial cells (dotted arrow) and enlarged, pale lens fibers throughout in the the Pex7 $^{neo/neo}$ compared to Pex7 $^{neo/+}$ lens. (E, F) Skeletal mounts at P1 show delayed ossification of the talus (ankle) and last middle phalange in the Pex7 $^{neo/neo}$ mice compared to Pex7 $^{neo/+}$. Alizarin red stains bone and alcian blue stains cartilage.

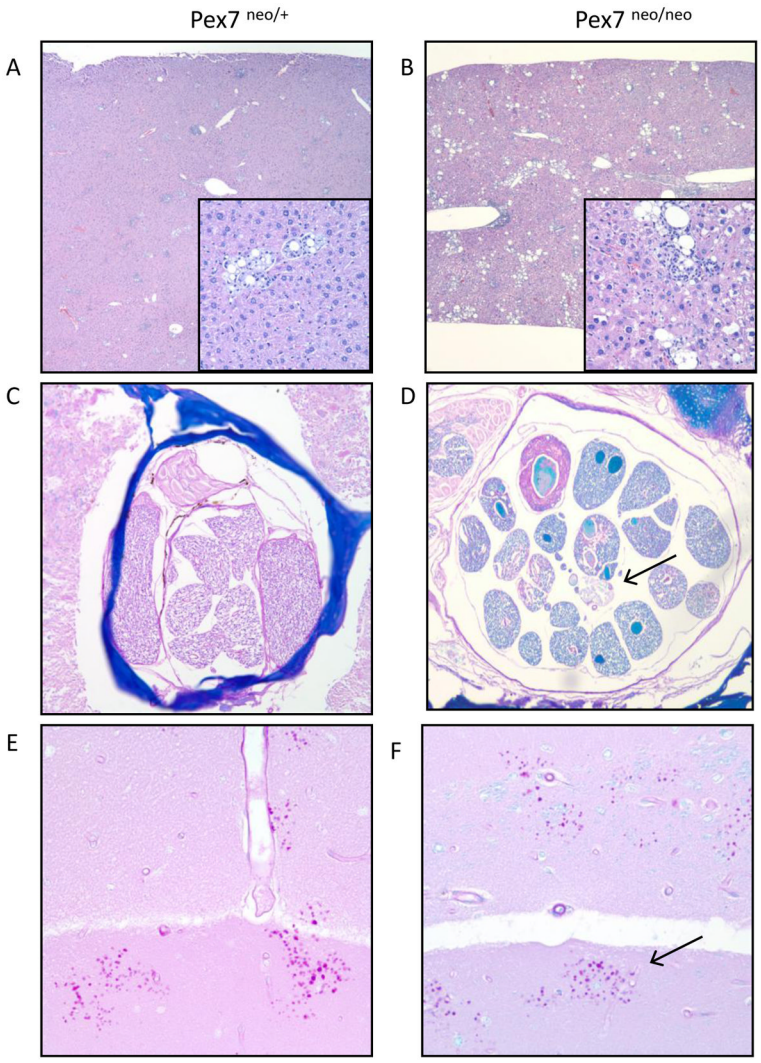

Fig. 7.

(A, B) H & E stained liver at 4x, with insert 40x magnification. Pex7 $^{neo/+}$ shows minimal diffuse hepatocellular changes, with periportal aggregates of lipid laden cells seen at 40x. Pex7 $^{neo/neo}$ liver shows more extensive vacuolation, microvesiculation and degenerative changes. (C, D) LFB/PAS stained transverse sections of cauda equina from Pex7$^{neo/+}$ mouse at 20x and Pex7 $^{neo/neo}$ at 10x magnification. At the arrow, there is reduced LFB stain in a spinal rootlet. (E, F) LFB/PAS stain of hippocampus at10x. Intraneural PAS positive granules (arrow) are more frequent in Pex7 $^{neo/neo}$ compared to Pex7 $^{neo/+}$ mouse.

Table 1

Peroxisome functions in Pex7 $^{neo/neo}$ mice

Plasmalogen levels[a]	**Pex7$^{neo/neo}$**	**Pex7$^{neo/+}$**
RBC (n=15)	1.09 (±0.17) [b]	2.27 (±0.38)
Brain (n=3)	3.08 (±0.30)	8.31 (±1.05)
Heart (n=3)	1.15 (±0.42)	4.11 (±0.18)
Lens epithelial cells (n=5, pooled)	0.54	1.55
Liver (n=3)	0.31 (±0.11)	0.38 (±0.25)
DHA levels in RBCs (umol/L RBC) (n= 7)	278.99 (±57.37)	419.86 (108.76)
Plasmalogen biosynthesis[c]		
Embryonic fibroblasts (n=2)	1.33 (±0.13)	0.71(±0.08)
Phytanic acid oxidation[d]		
Embryonic fibroblasts (n=2)	280.3 (±64.33)	374.62 (±47.38)

[a] C16:0, C18:0 and C18:1 DMA, expressed as % of total fatty acids

[b] mean and STD, $p < 0.05$ except in liver, p=0.7 (sample means compared by student T test, parameters were 2 tailed, unequal variance)

[c] 3H:14C ratio of ER: peroxisomal steps in plasmalogen biosynthesis, the smaller the ratio the greater the peroxisomal contribution.

[d] Oxidation of [1–14C] phytanic acid in pmol/48hours/mg protein

Table 2

Phytanic, pristanic acid and total fatty acid levels in mice supplemented with phytol.

	0.5% phytol supplementation [a]	
Tissue levels of phytanic acid (expressed as % of total fatty acids)	Pex7 $^{neo/neo}$	Pex7 $^{neo/+}$
Brain (n=1)	3.46	0.04
Heart (n=1)	9.26	0.75
Liver (n=1)	25.19	0.45
Plasma (n=10)	10.41 (±8.70) [b] range 3–30	0.69 (±0.33) range 0.2–1.2
Plasma levels of phytanic, pristanic and saturated fatty acids (uM)		
Phytanic acid (n=10)	733.27 (±753.76) range 224–2827	73.76 (±36.10) range 26–140
Pristanic acid (n=10)	2.8 (± 3.0)	4.1 (± 3.5)
Total saturated FA (n=4)	1473.21(± 230.38)	1940.26 (±300.52)

[a] Dietary phytol is converted endogenously to phytanic acid

[b] mean and STD, $p < 0.05$ except for pristanic acid $p=0.71$ (sample means compared by student T test, parameters were 2 tailed, unequal variance)

Table 3

Recovery of RBC plasmalogens, DHA, and fatty acids on batyl alcohol supplementation

	Plasmalogens			DHA	Fatty acids		
umoles/L RBCs	**C16:0DMA**	**C18:0DMA**	**C18:1DMA**	**C22:6n-3**	**C16:0**	**C18:0**	**C18:1**
no treatment (n=2)							
Pex7 $^{neo/neo}$	17.58	13.09	4.98	38	1083	537	333
Pex7 $^{neo/+}$	75.2	50.97	17.29	82	1543	797	446
batyl alcohol (n=2)							
Pex7 $^{neo/neo}$	41.05	33.71	12.11	181	1933	960	633
Pex7 $^{neo/+}$	86.05	65.33	22.83	106	1833	887	615